Fusion Engineering and Design
Volume 130, May 2018, Pages 48-55 - DOI: 10.1016/j.fusengdes.2018.03.030

Thermo-hydraulic analysis of EU DEMO WCLL breeding blanket

Emanuela Martelli[a], Gianfranco Caruso[a], Fabio Giannetti[a], Alessandro Del Nevo[b]

[a]*DIAEE, Sapienza University of Rome, Corso Vittorio Emanuele II, 244, 00186, Roma, Italy*
[b]*ENEA FSN-ING-PAN, ENEA CR Brasimone, Località Brasimone, 40032, Camugnano (BO), Italy*

In the frame of EUROfusion Work Package Breeding Blanket, thermal-hydraulic engineering analyses were carried out at ENEA Brasimone, in close cooperation with Sapienza University of Rome, to investigate thermal and fluid-dynamic behavior of the Water Cooled Lithium Lead Breeding Blanket, which is a candidate option for the European DEMO nuclear fusion reactor.

The research activity focused on the equatorial elementary cell of an outboard segment to investigate thermal field of breeding blanket and to evaluate breeding zone and first wall systems cooling ability. A three-dimensional finite volume model of the breeding unit was developed, adopting the commercial CFD code ANSYS CFX 15.0. Steady state simulations were carried out considering a heat flux of 0.5 $MW \cdot m^{-2}$, a radial power density distribution applied to all domains, and buoyancies forces activated in PbLi region. Results show that FW and BZ systems have good cooling efficiency, maintaining the maximum temperature in PbLi and solid structures well below 500 °C. The thermal-hydraulic results are discussed, highlighting open issues and suggesting pertinent modifications to DEMO WCLL coolant system layout aimed at optimizing the design.

Keywords: DEMO, WCLL blanket, Thermal-hydraulics, CFD

1. Introduction

The breeding blanket is a key component in a fusion power plant in charge of ensuring tritium breeding self-sufficiency, adequate neutron shielding and energy extraction for an efficient power conversion cycle.

The Water Cooled Lithium-Lead (WCLL) blanket has been identified as a feasible blanket candidate for DEMO fusion power plant and it is investigated in the EUROfusion Breeding Blanket Project [1] by ENEA and its linked third parties [2].

The WCLL blanket uses reduced activation ferritic-martensitic steel (Eurofer) as structural material, filled with Lithium-Lead (PbLi) as breeder, neutron multiplier and tritium carrier, and water at typical Pressurized Water Reactor (PWR) conditions as coolant.

Thermal and fluid-dynamic analyses have been carried out to obtain a complete temperature map of WCLL breeding blanket, to investigate PbLi flow path in breeding zone and to evaluate thermal-hydraulic efficiency of Breeding Zone (BZ) and First Wall (FW) coolant systems, verifying that maximum temperature of Eurofer structures is below 550 °C. The analyses focused on the equatorial breeding unit of an outboard segment [2]. A detailed three-dimensional finite volume model of the breeding unit is developed, adopting the commercial CFD code ANSYS CFX 15.0. This approach allows obtaining a temperature distribution in solid and fluid domains. Some steady state

author's email: emanuela.martelli@uniroma1.it

simulations are carried out in order to evaluate the BZ and FW cooling ability and to optimize the temperature distribution changing system layout.

2. WCLL breeding blanket design

The WCLL BB design is based on DEMO 2015 specifications [3] and CAD model, which is characterized by 18 sectors. Each sector (20°) includes two inboard segments and three outboard segments.

Starting from the main outcomes obtained from WCLL 2015 design and analyses [4][5][6], an advanced and optimized design has been developed in 2016. The WCLL blanket concept [2] is based on the Single Module Segment (SMS) approach. The blanket segment, shown in Fig. 1, consists of an external box, composed by the First Wall (FW), directly exposed to the plasma, the Side Walls (SWs), the bottom and top caps and the Back Plate (BP).

The blanket segment is reinforced with a set of stiffeners: radial-toroidal stiffeners divide the segment in poloidal direction in slices (i.e. breeding units) illustrated in detail in Fig. 1 and Fig. 2. Five radial-poloidal stiffeners divide the breeding units in 6 toroidal channels, where PbLi is distributed. A baffle plate, placed at half between two horizontal stiffeners, ensures the circulation of PbLi in radial-poloidal direction inside the breeding zone (see Fig. 3). The breeding units are filled with PbLi alloy and cooled by means of water, at PWR conditions, flowing in radial-toroidal Double Wall Tubes (DWTs) crossing vertical stiffeners. The FW and SWs are cooled by means of square channels, where water flows in counter-current direction at PWR conditions.

In order to transfer the thermal power to the Power Conversion System (PCS) [7], the WCLL blanket is linked and integrated with the Primary Heat Transfer System (PHTS) [2] through the in-vessel piping system, which is formed by the feeding and collecting pipes of the inboard and outboard segments.

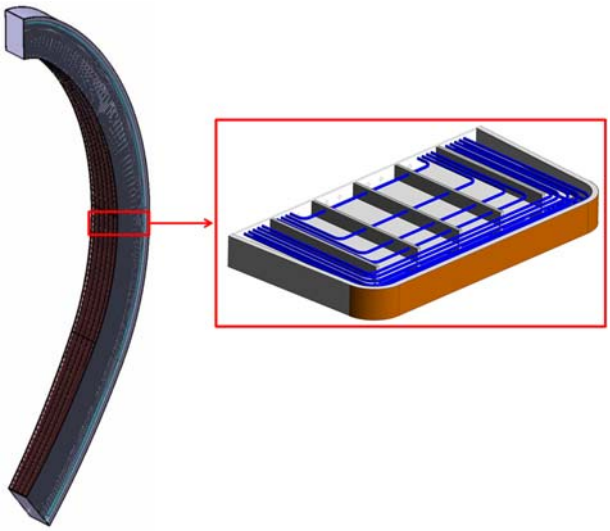

Fig. 1. WCLL BB 2016 design: outboard segment and breeding unit at equatorial plane.

Fusion Engineering and Design
Volume 130, May 2018, Pages 48-55 - DOI: 10.1016/j.fusengdes.2018.03.030

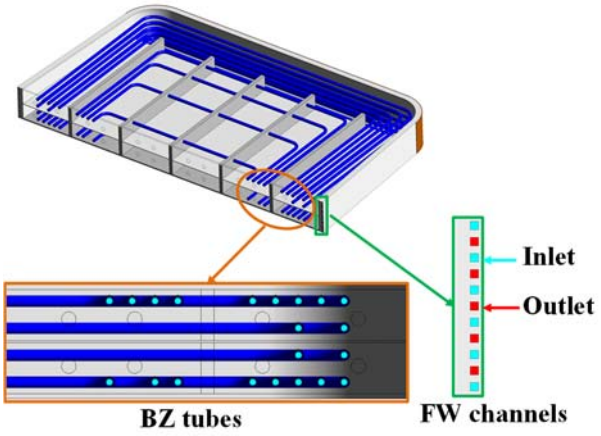

Fig. 2. WCLL breeding unit: detail of FW and BZ coolant systems.

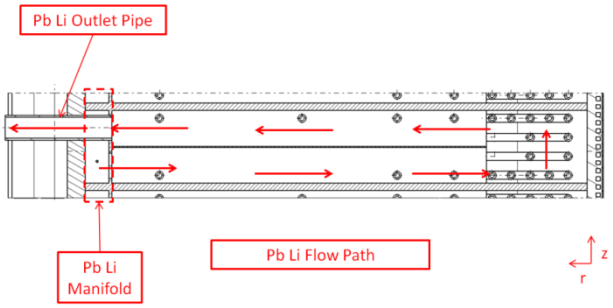

Fig. 3. WCLL breeding unit: PbLi flow path.

3. Computational model

3.1 Geometry

A three-dimensional finite volume model of the breeding unit of DEMO WCLL blanket was set-up, using ANSYS CFX v15.0 code. The model includes solid domains (i.e. stiffeners, DWTs, FW, and Tungsten layer) and fluid domains (i.e. PbLi and water coolant), schematized in Fig. 4.

The breeding unit has an average toroidal distance of 1300 mm, the radial dimension is 827 mm and the total height is 135 mm. The model is developed considering half height of radial-toroidal stiffeners, as the periodic condition is applied. The BZ coolant system consists of 21 DWTs with hydraulic diameter of 8 mm and an external diameter of 13.5 mm. The gap of DWT is not modeled. The breeding unit includes 10 square channels in the FW of 7×7 mm.

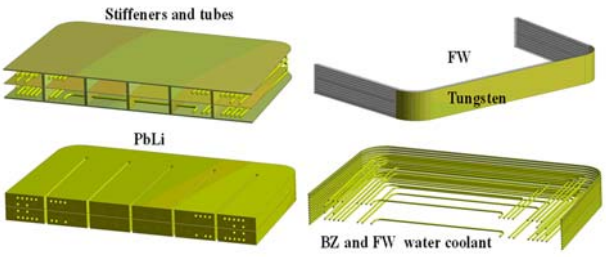

Fig. 4. CFX solid domains (i.e. stiffeners, DWTs, FW and tungsten layer) and fluid domains (i.e. PbLi, FW and BZ coolant).

3.2 Mesh

A mesh independency analysis, described in Ref. [8], is performed for the finite volume model to select optimized spatial discretization, allowing accurate results and reasonable calculation time. A first preliminary independent analysis is conducted on BZ and FW fluid domains. For this purpose, simulations are carried out for one BZ tube and one FW single channel, using meshes with different degree of detail. Pressure drops between inlet and outlet and the bulk temperature are evaluated for each case and compared with the others, as reported in Tab. 1 and Tab. 2.

The analysis demonstrated that a good comprise between accuracy and computational cost is achieved with 1.43×10^6 nodes in one FW channel and 1.78×10^6 nodes in one BZ tube.

Once selected the mesh for BZ and FW water domains, a sensitivity analysis is conducted using the complete computational model. Three meshes are set-up which differ for the level of detail in the PbLi domain as well as in the solid structures. The parameters used for the comparison are the maximum and the outlet temperature of PbLi domain. The results, reported in Tab. 3, showed that a good compromise between degree of detail and the computational time efforts is achieved with a minimum of 10.3×10^6 nodes.

Tab. 1. FW single channel mesh grid details and results.

Mesh	N. nodes	ΔP [Pa]	T [°C]
A	45632	6349	314.61
B	59520	6352	314.90
C	87296	6380	315.16
D	142848	6500	315.29
E	244528	6505	315.40

Tab. 2. BZ single tube mesh grid details and results.

Mesh	N. nodes	ΔP [Pa]	T [°C]
A	36296	4450	308.10
B	91438	5201	310.60
C	124244	5315	310.72
D	**178688**	**5453**	**311.32**
E	256166	5549	311.34

Tab. 3. Computational domain mesh grid details and results.

Mesh	N. nodes	PbLi T_{max} [K]	PbLi T_{out} [K]
C1	8.2×10^6	544.85	310.86
C2	10.3×10^6	548.46	314.92
C3	12.8×10^6	548.57	315.25

The selected mesh, used for the simulations, is characterized by 14×10^6 nodes and 28×10^6 elements. Hexahedral and tetrahedral elements are adopted to discretize the model, considering the geometrical features of the domains to be meshed and the required optimization of the node number and mesh quality. Mesh statistics information are

Fusion Engineering and Design
Volume 130, May 2018, Pages 48-55 - DOI: 10.1016/j.fusengdes.2018.03.030

summarized in Tab. 4. In particular, structured hexahedral mesh is adopted in the BZ and FW coolant domain, and solid structures, as shown in Fig. 5. Inflation layers at the coolant-solid interface are used for the resolution of the viscous sub-layer. The mesh follows the channel profile in radial-toroidal direction. Tetrahedral elements in the PbLi domain with inflation layers at the PbLi-solid structures interface are used, to allow a better description of the system, as those regions require more detail due to higher velocity gradients.

Tab. 4. Mesh statistics.

Parameter	Value
Nodes	14×10^6
Elements	28×10^6
Average Skewness	0.2938
Average Orth. Quality	0.831

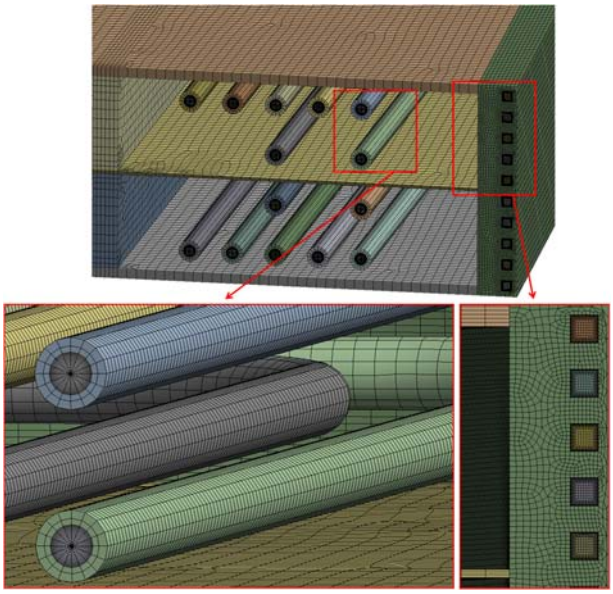

Fig. 5. Mesh of CFD model: detail of BZ and FW coolant, and Eurofer structures.

3.3 Solver settings

The Reynolds Averaged Navier Stokes (RANS) equations have been solved for the single-phase fluid domains, using the k-ω Shear Stress Transport (SST) turbulence model, in order to account for the turbulence generated in the water domains, without losing accuracy in the free stream. The

Periodic condition is imposed on the upper and lower surfaces of radial-toroidal plates, FW and tungsten layer, to simulate the presence of the others breeding units. Adiabatic condition is applied to SWs, to back walls of PbLi, FW, tungsten and tubes. Thermal conduction is enabled in all solid domains, allowing the heat transfer between the solid structures and between solid and fluid domains.

Concerning the PbLi breeder, buoyancy forces are considered in PbLi domain, thus the heat transfer between fluid domains occurs by means convection and conduction phenomena

The material physical properties have been implemented in CFX code database. The physical properties of solid domains (i.e. Eurofer and Tungsten) are specified in terms of density, specific heat and thermal conductivity, while fluid domains (i.e. water and PbLi) require also the dynamic viscosity. The relevant material properties of Eurofer, Tungsten and PbLi are summarized in the Appendix.

3.4 Heat loads

The FW surface is subjected to a power deposition due to particles and radiations arising from plasma. This is modelled with a maximum nominal heat flux of 0.5 $MW \cdot m^{-2}$, imposed onto the straight surface of the FW, and, concerning the SWs, a cosine-dependent law has been adopted for them [9].

Moreover, a radial distribution of heat power density is applied to the model (i.e. solid structures and PbLi domains) to simulate power deposited by neutrons and photons.

The volumetric power density is based on the neutronic calculations carried out for the past PPCS-A WCLL blanket design [10], scaled with the 2015 DEMO1 average neutron wall load [3] and integrated with the radial model of the WCLL blanket design [9]. The radial distribution of the heat power density in Eurofer and PbLi is reported in Fig. 6. The volumetric generation in the coolant is neglected in the model.

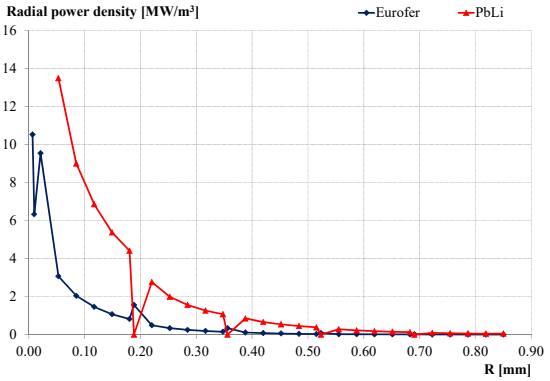

Fig. 6. Radial power density distribution of outboard segment.

4. CFD simulations

Steady state CFD simulations have been carried out to evaluate the thermal behaviour of breeding unit, verifying that solid structures temperature is below the limit (550 °C) and investigating cooling ability of BZ and FW systems. A summary of simulations performed is summarized in Tab. 5.

Tab. 5. CFD simulations.

#	Description	Note
1	FW mflow: 37% of total mflow BZ mflow: 63% of total mflow	Mass flow rate calculated with enthalpy balance

2	FW mflow: 45% of total mflow BZ mflow: 55% of total mflow	Mass flow rate obtained from TM analyses
3	FW mflow: 45% of total mflow BZ mflow: 55% of total mflow	Counter-current flow adopted in BZ system
4	FW mflow: 37% of total mflow BZ mflow: 63% of total mflow	Recirculation adopted in BZ system

Taking into account thermal loads discussed in Section 3.4, the total power in the breeding unit is 0.346 MW, of which 0.127 MW are deposited in the FW and 0.219 MW in the BZ. Thus, assuming that water enters in both coolant systems at 285 °C and exits at 325 °C, at 15.5 MPa, the total mass flow rate needed to extract the thermal power is 1.529 kg·s^{-1}. The PbLi inlet mass flow rate is 0.14 kg·s^{-1}, at 325 °C of temperature. The inlet boundary conditions are summarized in Tab. 6.

Tab. 6. CFX model boundary conditions.

Parameter	Units	Value
FW HF (max)	MW m^{-2}	0.5
Total Power		0.346
BZ	MW	0.127
FW		0.219
Coolant (BZ-FW) T_{inlet}	°C	285
Coolant (BZ-FW) Pressure	MPa	15.5
PbLi T_{inlet}	°C	325
PbLi Mass Flow	kg/s	0.146

In Case 1 and Case 2 the water coolant of BZ system enters in the right side of the breeding unit and exits from the left side, flowing in radial-toroidal direction, as indicated in Fig. 7. Assuming the same total mass flow rate (1.529 kg/s), the two simulations differ for the mass flow rate distribution between FW and BZ coolant systems.

In Case 1 the FW mass flow rate is 37% of total mass flow rate, and the BZ mass flow rate is 63%. The mass flow rate of each system is calculated with the enthalpy balance, taking into account the power deposited in the system and water thermo-dynamic cycle (285-325 °C). Equal inlet mass flow is assumed in FW channels, instead BZ mass flow is distributed in the tubes depending upon tube length and the nuclear heating deposited near the tube.

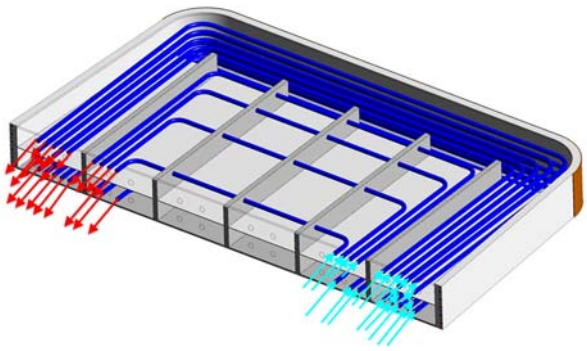

Fig. 7. Case 1 and Case 2 BZ coolant system layout: blue rows indicate water inlet; red rows indicate water outlet.

In Case 2, a mass flow rate distribution based on thermo-mechanical (TM) results [11] has been considered in the CFD model. The FW and BZ mass flow rates are, respectively, 45% and 55% of total mass flow. In Tab. 7 the mass flow rates of each BZ tube are reported: the tubes are labelled from 1 to 9 in toroidal direction, starting from the first line near the right SW and from 1 to 4 in poloidal direction (i.e. 1_1).

Tab. 7. BZ mass flow rate.

#	BZ tubes	Mass flow rate [kg/s]
1	1_1; 1_2; 1_3; 1_4	0.0736
2	2_1; 2_4	0.0502
3	3_1; 3_2; 3_3, 3_4	0.0441
4	4_1; 4_4	0.0336
5	5_1; 5_4	0.0419
6	6_1; 6_4	0.0383
7	7_1; 7_4	0.0264
8	8_1	0.0199
9	9_1; 9_4	0.0046

In Case 3, a counter-current flow path was simulated, as schematized in Fig. 8, assuming the same mass flow rate distribution of Case 2.

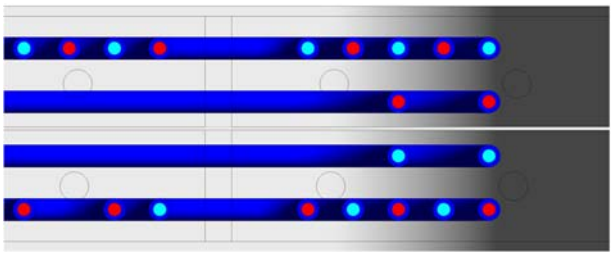

Fig. 8. Case 3, BZ coolant system layout: inlet (blue) and outlet (red) orifices

Finally, in Case 4, BZ water enters in the 10 tubes near the FW, flows in radial-toroidal direction, it is collected in a manifold and then recirculates into the other 11 tubes in the opposite direction, as represented in Fig. 5. The same mass flow rate distribution of Case 1 is assumed for BZ and FW systems, and equal flow is assumed at BZ tubes inlet.

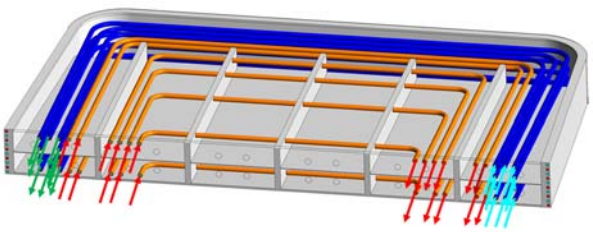

Fig. 9. Case 4, BZ coolant system layout.

Fusion Engineering and Design
Volume 130, May 2018, Pages 48-55 - DOI: 10.1016/j.fusengdes.2018.03.030

5. Results and discussions

5.1 Results

A detailed analysis of the results is performed and hereafter discussed. Considering Case 1, the outlet temperature of water in FW and BZ is 329.1 °C and 322.2 °C, respectively. The outlet temperature is obtained from the CFX post [12] as the temperature averaged on the local mass flow rate and on the overall outlet tube sections.

The results demonstrate that, being the FW outlet temperature greater than theoretic value (325 °C), and the BZ outlet temperature lower, the FW coolant system extracts part of the power of the BZ system. The comparison between the power deposited and the power extracted by FW and BZ systems confirms this result. The difference between the power deposited and the power extracted in the FW coolant system is equal to 12.72% and in the BZ coolant system is -7.86%. This phenomenon is correlated to the radial profile of the volumetric power density, which is higher in the region near the FW. The analysis demonstrates that the calculation of mass flow distribution between the two systems cannot be based only on the enthalpy balance, thus a sensitivity analysis is performed to improve coolant systems efficiency.

The pressure drop has been calculated directly by taking the inlet and outlet pressures. The pressure drop in the BZ system is 0.9626×10^4 Pa, which is the maximum value achieved in the longest tube. The pressure drops in FW channels are characterized by few variations and the average value is 0.7418×10^4 Pa.

As regard the breeding region, Case 1 presents a maximum temperature of 414.8 °C in Eurofer domain, which is well below the maximum allowable value (550 °), as shown in Fig. 10.

Nevertheless, it was noted an asymmetric temperature distribution in toroidal direction in PbLi and Eurofer domains, as illustrated in Fig. 10 and Fig. 11, where PbLi and solid structures temperature map is reported, respectively. This asymmetry is mainly due to the BZ coolant system layout, as cold water enters in the right side of the breeding unit and hot water exits from left side. The toroidal asymmetry is an issue, as it is source of thermal stress for the Eurofer structures. Moreover, the toroidal asymmetry determines the presence of two regions with different PbLi density and, due to the buoyancy forces, there is a PbLi net flow in toroidal direction in addition to the dominant radial-poloidal flow.

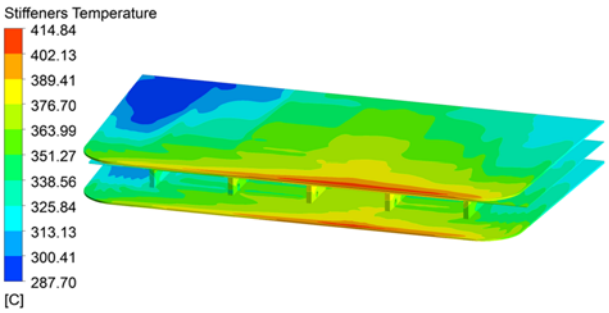

Fig. 10. Case 1: stiffeners temperature distribution.

Fusion Engineering and Design
Volume 130, May 2018, Pages 48-55 - DOI: 10.1016/j.fusengdes.2018.03.030

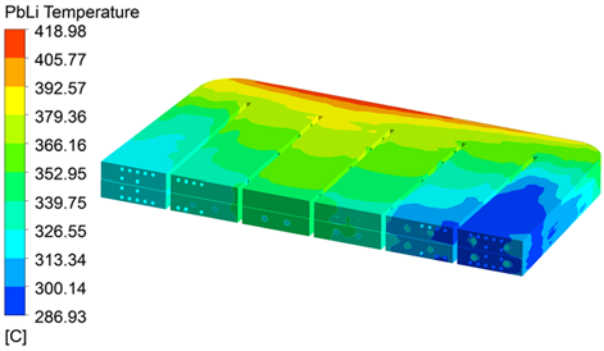

Fig. 11. Case 1, PbLi temperature distribution.

Taking into account the outcomes from Case 1, a sensitivity analysis is performed (Case 2) considering a different mass flow rate distribution as described in Section 4. The results of Case 2 show a better distribution of outlet temperature in the two coolant systems: the average coolant outlet temperature is 323.5 °C in the FW and 324.7 °C in BZ coolant system. The water temperature variation with respect the theoretic value (325 °C) implies a thermal imbalance in PbLi domain which implies an increase of outlet temperature of 63 °C, and thus it is equal to 387.8 °C. Moreover, it is noted that the PbLi outlet temperature computed by the code (i.e. temperature averaged on the local mass flow rate) is lower and equal to 359.5 °C. This is due to the asymmetric thermal field that, as enlightened before, determines an additional PbLi net flow in toroidal direction which involves the entry of cold PbLi from the outlet orifices.

FW Eurofer maximum temperature is reduced with respect previous case, as indicated in Tab. 8, where maximum and minimum temperatures of all domains (i.e. solid and fluids) are reported. Fig. 12 illustrates the thermal field of FW Eurofer structure: the counter-current flow of water coolant ensures the temperature symmetry in toroidal direction.

Considering that the average coolant velocity is 1.3 m/s in the BZ system and 2.0 m/s in FW system, which is well below the assumed limit (7 m/s), there is margin to further improve cooling performances.

As regard PbLi and Eurofer domains, Case 2 present a similar thermal field of Case 1, the difference between maximum temperatures is about 1 °C. The temperature in solid structures remain well below the Eurofer maximum allowable value (550 °C) in both simulations.

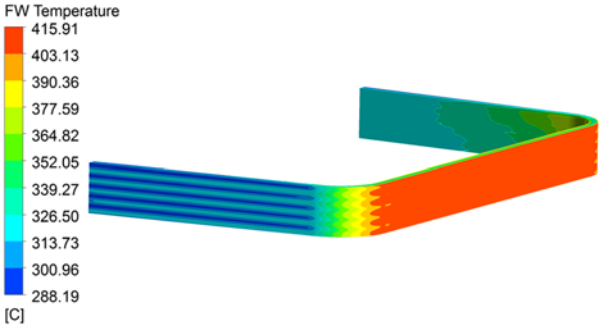

Fig. 12. Case 2: FW Eurofer thermal field.

In order to achieve a temperature symmetry in toroidal direction two alternative BZ coolant system layouts have been investigated, as described in previous Section.

Fusion Engineering and Design
Volume 130, May 2018, Pages 48-55 - DOI: 10.1016/j.fusengdes.2018.03.030

The results of CFD simulation of Case 3 show that this configuration ensures temperature symmetry in toroidal direction. A radial-toroidal view of PbLi thermal field domain is reported in Fig. 13. The maximum temperature of Eurofer stiffeners is 417.2 °C, which is still below 500 °C, as shown in Fig. 14. Moreover, a good outlet temperature distribution is achieved in BZ coolant system with an average outlet temperature of 325.8 °C, as reported in Tab. 8.

Nevertheless, the counter-current flow in BZ system requires water (inlet and outlet) manifolds that are difficult to be integrated with current design, considering the available space between the back plate and the BSS and constraints of DEMO 2015 specifications.

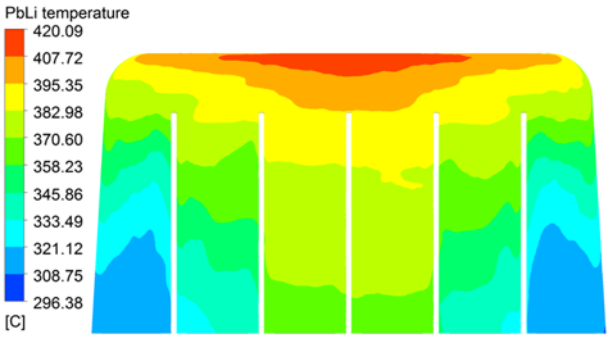

Fig. 13. Case 3, radial-toroidal view of PbLi temperature distribution.

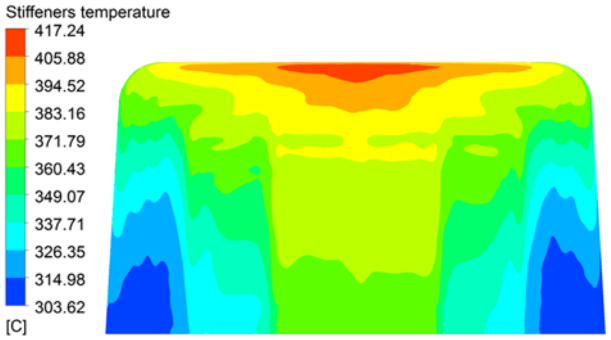

Fig. 14. Case 3, radial-toroidal view of stiffeners temperature distribution.

Finally, in Case 4 BZ coolant system layout is modified as indicated in Fig. 9. The results of the analyses show that the symmetry of thermal field in toroidal direction is improved with respect Case 1 and Case 2, even if it can be further improved. The thermal field of PbLi and solid structures, reported in Fig. 15 and Fig. 16, respectively, presents lower temperature in the right side of the breeding unit where cold water enters in the BZ coolant system.

As regard BZ coolant system, outlet temperature is more homogenous and maximum temperature is reduced, as demonstrated in Tab. 8 and Fig. 17, where the temperature of BZ coolant is reported. The maximum value indicated in Fig. 17 is greater than the value in Tab. 8 as the table reports bulk temperatures, instead the figure shows the temperature at the interface coolant/tube. The BZ coolant efficiency is enhanced, as water velocity is increased (2.67 m/s) and the maximum temperature of Eurofer stiffeners (408 °C) is decreased with respect previous cases, which is shown in Fig. 16. Nevertheless, as in Case 1, the outlet temperature of BZ and FW coolant is affected by the mass flow rate distribution calculated considering only the enthalpy balance.

Fusion Engineering and Design
Volume 130, May 2018, Pages 48-55 - DOI: 10.1016/j.fusengdes.2018.03.030

The pressure drop in the BZ system is increased with respect Case 1 and it is equal to 1.656×10^4 Pa. There are no variations of pressure drop in the FW coolant system.

5.2 Main achievements

The CFD analyses carried out demonstrated that the WCLL has a good thermal behavior, with maximum temperature of PbLi and Eurofer domains always below 500 °C. The analysis performed in Case 1 highlight that mass flow rate distribution shall be evaluated taking into the effective power deposited in FW and BZ systems, which depends from radial profile of volumetric power density.

An asymmetric temperature distribution is evidenced in Case 1 and Case 2, due to the BZ coolant system layout, thus sensitivity analyses are performed to optimize the thermal field in PbLi and Eurofer domains. The BZ coolant system layout, presented in Case 4, is the only configuration that can be integrated successfully with current WCLL design, as the counter-current flow in BZ system (Case 3) requires water (inlet and outlet) manifolds that are difficult to be integrated with current design.

Further studies [13] are needed and alternative configurations should be investigated, to improve temperature symmetry in toroidal direction, and to simplify the design (i.e. avoiding pipes crossing vertical stiffeners).

Moreover, being the BZ and FW coolant velocity below the assumed limit (7 m/s) there are margins to reduce number of tubes and to increase coolant systems efficiency.

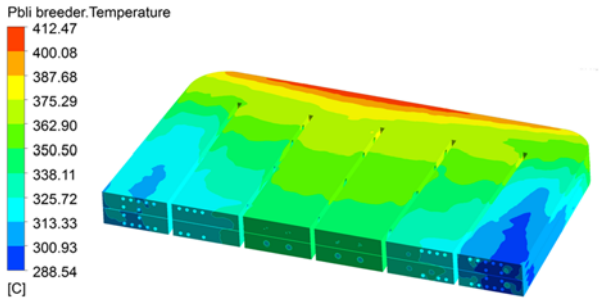

Fig. 15. Case 4, PbLi temperature distribution.

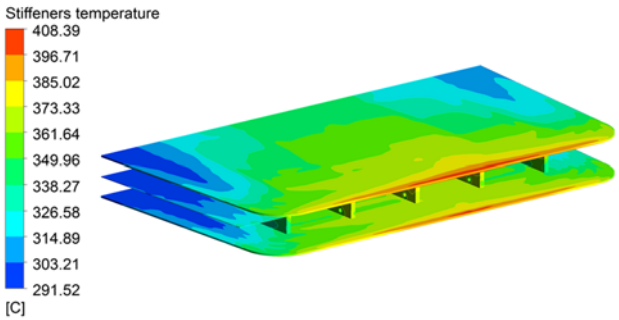

Fig. 16. Case 4 stiffeners temperature distribution.

Fusion Engineering and Design
Volume 130, May 2018, Pages 48-55 - DOI: 10.1016/j.fusengdes.2018.03.030

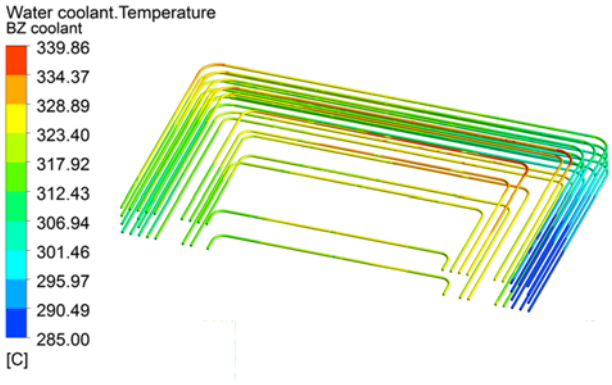

Fig. 17. Case 4, BZ coolant temperature at coolant-tube interface

Tab. 8. Temperature in solid and fluid domains.

#	Description	Case 1	Case 2	Case 3	Case 4
	PbLi				
1	T_{min} [°C]	286.9	286.8	296.85	288.7
	T_{max}[°C]	418.9	417.3	420.05	412.4
	Eurofer structures				
2	T_{min} [°C]	287.6	287.6	304.35	291.5
	T_{max}[°C]	414.8	413.1	417.25	408.3
	FW Eurofer				
3	T_{min} [°C]	289.4	288.3	286.05	289.25
	T_{max} [°C]	425.4	415.8	422.25	424.9
	Tungsten				
4	T_{min} [°C]	312.7	308.6	304.85	312.5
	T_{max} [°C]	433.2	423.6	434.15	432.8
	BZ coolant				
5	T_{min} [°C]	284.9	284.9	284.95	284.9
	T_{max} [°C]	332.7	339.5	343.45	330.4
	FW coolant				
6	T_{min} [°C]	284.9	284.9	284.95	284.9
	T_{max} [°C]	Sat	342.0	344.75	Sat
7	BZ coolant avg T_{out} [°C]	322.2	324.7	325.8	322.4
8	FW coolant avg T_{out} [°C]	329.1	323.5	323.4	328.1

Minimum and maximum temperature are bulk values

6. Conclusions

Within the frame of EUROfusion Power Plant Physics & Technology Work Programme research activities have been carried out to investigate thermal and fluid-dynamic performances of DEMO WCLL breeding blanket concept. The analyses, based on WCLL 2016 design, focused on the breeding unit of an outboard segment. A computational thermal and fluid-dynamic model of the breeding unit was developed adopting the commercial CFD code ANSYS CFX 15.0.

The results of the CFD simulations demonstrated that WCLL blanket concept has good thermal behavior with margins to further enhance the coolant systems performances, optimizing BZ layout and simplifying the design. In particular, the following outcomes arise from the analyses:

- The coolant systems efficiency is satisfactory, ensuring a maximum temperature of PbLi and stiffeners always below 500 °C. Moreover, considering that the average velocity of coolant systems is well below the assumed limit (7 m/s), the efficiency can be further improved (i.e. reducing overall tubes length).
- Mass flow rate distribution shall be evaluated considering that FW coolant system extracts part of BZ coolant system power. Further iterations are needed to optimize temperature distribution.
- The thermal field in the breeding zone presents an asymmetric toroidal temperature distribution, due to the BZ coolant system layout, which is based on 2015 design. Two alternative configurations have been studied and discussed. Case 3 considers a counter-current flow in BZ system demonstrating the possibility of achieving temperature symmetry in toroidal direction Nevertheless, this configuration cannot be integrated in the manifold region. In Case 4 the coolant recirculates in the BZ system, showing an improved toroidal symmetry of temperature distribution with respect Case 1 and 2. The last configuration is the only cooling scheme that can be integrated with current design. Further analyses are needed to improve BZ thermal field, taking into account design constraints.

Appendix

The material thermo-physical properties have been implemented in CFX uniquely as a function of temperature, using a polynomial fitting of data. The data summarized in Tab. 9 and Tab. 10, have been employed for Eurofer and Tungsten material, respectively.

As regard PbLi alloy, properties are summarized in Tab. 11 The PbLi dynamic viscosity (μ) is implemented according with the following equation (1) [15]:

$$\mu_{PbLi} = 1.87 \cdot 10^{-4} \cdot e^{\frac{11640}{T \cdot R}} [Pa \cdot s] \quad (1)$$

Tab. 9. Thermo-physical properties of Eurofer [14].

T [°C]	ρ [kg m^{-3}]	C_p [J kg^{-1} K^{-1}]	λ [W m^{-1} K^{-1}]
20	7750	448	28.3
100	7728	486	29.2
200	7699	522	30.7

300	7666	551	30.2
400	7633	584	29.3
500	7596	655	29.5
600	7558	801	31.2

Tab. 10. Thermo-physical properties of Tungsten [9].

T [°C]	ρ [kg m^{-3}]	C_p [J kg^{-1} K^{-1}]	λ [W m^{-1} K^{-1}]
20	19298	129.0	172.8
100	19279	131.6	164.8
200	19254	134.7	155.5
300	19229	137.8	147.2
400	19205	140.9	139.8
500	19178	143.9	133.1
600	19152	146.8	127.2
700	19125	149.6	122.1

Tab. 11. Thermo-physical properties of PbLi [15].

T [°C]	ρ [kg m^{-3}]	C_p [J kg^{-1} K^{-1}]	λ [W m^{-1} K^{-1}]
20	10172	192	7.69
300	9839	190	13.18
350	9779	189	14.16
400	9720	189	15.14
450	9661	188	16.12
500	9601	188	17.10
550	9542	187	18.08
600	9482	187	19.06
650	9423	187	20.04
700	9363	186	21.02

Acknowledgments

This work has been carried out within the framework of the EUROfusion Consortium and has received funding from the Euratom research and training programme 2014-2018 under grant agreement No 633053. The views and opinions expressed herein do not necessarily reflect those of the European Commission.

References

[1] G. Federici, et al., Overview of the design approach and prioritization of R&D activities towards an EU DEMO, Fusion Eng. and Des., 109–111 (2016), pp. 1464-1474.

[2] E. Martelli, et al, Advancements in DEMO WCLL breeding blanket design and integration. Int. J. Energy Res., 42 (2018) pp. 27–52.

[3] H. Hurzlmeier, B. Meszaros, EU DEMO1 2015 - DEMO_TOKAMAK_COMPLEX, 2M9AJJ, 08 May 2015.

[4] A. Del Nevo, et al., WCLL breeding blanket design and integration for DEMO 2015: status and perspectives, Fusion Eng. and Des., 124, (2017), pp. 682-686.

[5] R. Mozzillo, et al., Rationale and method for design of DEMO WCLL breeding blanket poloidal segmentation, Fusion Eng. Des., 124 (2016), pp. 664-668.

[6] E. Martelli, et al., Thermal-hydraulics CFD analysis of WCLL BB PbLi manifold, Fusion Eng. Des., 124 (2016), pp. 944-947.

[7] L. Malinowski, et al., Analysis of the secondary circuit of the DEMO fusion power plant using GateCycle, Fusion Eng. Des., 124 (2017), pp. 1237-1240.

[8] A. Del nevo et al., WCLL Design Report 2015, Eurofusion Internal deliverable, March 2016.

[9] A. Del Nevo et al., Design Description Document 2015 for WCLL (update of DDD 2014), IDM ref EFDA_D_2MU9XC v1.1.

[10] Y. Chen et al., The EU Power Plant Conceptual Study-Neutronic Design Analyses for Near Term and Advanced Reactor Models, 2003.

[11] P.A. Di Maio, et al., On the thermo-mechanical behaviour of DEMO water-cooled lithium lead equatorial outboard blanket module, Fusion Eng. Des., 124 (2017) pp.

[12] ANSYS CFX 15.0 Guide, November 2013.

[13] A. Tassone et al., Recent progress in the WCLL breeding blanket design for the DEMO fusion reactor, IEEE Transactions on Plasma Science, 99, 1-12, 2018

[14] Tavassoli, Fusion Demo Interim Structural Design Criteria (DISDC)/Appendix A Material Design Limit Data/A3. S18E Eurofer Steel, EFDA TASKTW4-TTMS-005-D01, CEA Report DMN/DIR/NT/2004-02/A, December 2004.

[15] E. Mas de les Valls et al., Lead-Lithium eutectic material database for nuclear fusion technology, Journal of Nuclear Materials 376 (2008) 353-357.